The Astrophysical Journal, 700:1059–1066, 2009 August 1 doi:10.1088/0004-637X/700/2/1059

PULSED GAMMA-RAYS FROM PSR J2021+3651 WITH THE *FERMI* LARGE AREA TELESCOPE

A. A. Abdo[1,54], M. Ackermann[2], M. Ajello[2], W. B. Atwood[3], L. Baldini[4], J. Ballet[5], G. Barbiellini[6,7], D. Bastieri[8,9], M. Battelino[10], B. M. Baughman[11], K. Bechtol[2], R. Bellazzini[4], B. Berenji[2], E. D. Bloom[2], G. Bogaert[12], A. W. Borgland[2], J. Bregeon[4], A. Brez[4], M. Brigida[13,14], P. Bruel[12], T. H. Burnett[15], G. A. Caliandro[13,14], R. A. Cameron[2], F. Camilo[16], P. A. Caraveo[17], J. M. Casandjian[5], C. Cecchi[18,19], E. Charles[2], A. Chekhtman[20,1], A. W. Chen[17], C. C. Cheung[21], J. Chiang[2], S. Ciprini[18,19], I. Cognard[22], J. Cohen-Tanugi[23], L. R. Cominsky[24], J. Conrad[10,25], S. Cutini[26], P. Demorest[27], C. D. Dermer[1], A. de Angelis[28], A. de Luca[29], F. de Palma[13,14], S. W. Digel[2], M. Dormody[3], E. do Couto e Silva[2], P. S. Drell[2], R. Dubois[2], D. Dumora[30,31], C. Espinoza[32], C. Farnier[23], C. Favuzzi[13,14], W. B. Focke[2], M. Frailis[28], P. C. C. Freire[33], Y. Fukazawa[34], S. Funk[2], P. Fusco[13,14], F. Gargano[14], D. Gasparrini[26], N. Gehrels[21,35], S. Germani[18,19], B. Giebels[12], N. Giglietto[13,14], F. Giordano[13,14], T. Glanzman[2], G. Godfrey[2], I. A. Grenier[5], M.-H. Grondin[30,31], J. E. Grove[1], L. Guillemot[30,31], S. Guiriec[23], Y. Hanabata[34], A. K. Harding[21], M. Hayashida[2], E. Hays[21], R. E. Hughes[11], G. Jóhannesson[2], A. S. Johnson[2], R. P. Johnson[3], T. J. Johnson[21,35], W. N. Johnson[1], S. Johnston[36], T. Kamae[2], H. Katagiri[34], J. Kataoka[37], N. Kawai[38,37], M. Kerr[15], B. Kiziltan[39], J. Knödlseder[40], N. Komin[5,23], M. Kramer[32], F. Kuehn[11], M. Kuss[4], J. Lande[2], L. Latronico[4], S.-H. Lee[2], M. Lemoine-Goumard[30,31], F. Longo[6,7], F. Loparco[13,14], B. Lott[30,31], M. N. Lovellette[1], P. Lubrano[18,19], A. G. Lyne[32], A. Makeev[20,1], R. N. Manchester[36], M. Marelli[17], M. N. Mazziotta[14], W. McConville[21], J. E. McEnery[21], M. A. McLaughlin[41], C. Meurer[25], P. F. Michelson[2], W. Mitthumsiri[2], T. Mizuno[34], A. A. Moiseev[42], C. Monte[13,14], M. E. Monzani[2], A. Morselli[43], I. V. Moskalenko[2], S. Murgia[2], P. L. Nolan[2], A. Noutsos[32], E. Nuss[23], T. Ohsugi[34], N. Omodei[4], E. Orlando[44], J. F. Ormes[45], M. Ozaki[46], D. Paneque[2], J. H. Panetta[2], D. Parent[30,31], M. Pepe[18,19], M. Pesce-Rollins[4], F. Piron[23], T. A. Porter[3], S. Rainò[13,14], R. Rando[8,9], S. M. Ransom[27], M. Razzano[4], A. Reimer[2], O. Reimer[2], T. Reposeur[30,31], S. Ritz[21,35], L. S. Rochester[2], A. Y. Rodriguez[47], R. W. Romani[2], F. Ryde[10], H. F.-W. Sadrozinski[3], D. Sanchez[12], P. M. Saz Parkinson[3], C. Sgrò[4], A. Sierpowska-Bartosik[47], E. J. Siskind[48], D. A. Smith[30,31], P. D. Smith[11], G. Spandre[4], P. Spinelli[13,14], B. W. Stappers[32], J.-L. Starck[5], M. S. Strickman[1], D. J. Suson[49], H. Tajima[2], H. Takahashi[34], T. Takahashi[46], T. Tanaka[2], J. B. Thayer[2], J. G. Thayer[2], G. Theureau[22], D. J. Thompson[21], S. E. Thorsett[3], L. Tibaldo[8,9], D. F. Torres[50,47], G. Tosti[18,19], A. Tramacere[51,2], Y. Uchiyama[2], T. L. Usher[2], A. Van Etten[2], N. Vilchez[40], V. Vitale[43,52], A. P. Waite[2], E. Wallace[15], K. Watters[2], P. Weltevrede[36], K. S. Wood[1], T. Ylinen[53,10], and M. Ziegler[3]

[1] Space Science Division, Naval Research Laboratory, Washington, DC 20375, USA
[2] W. W. Hansen Experimental Physics Laboratory, Kavli Institute for Particle Astrophysics and Cosmology, Department of Physics and Stanford Linear Accelerator Center, Stanford University, Stanford, CA 94305, USA
[3] Santa Cruz Institute for Particle Physics, Department of Physics and Department of Astronomy and Astrophysics, University of California at Santa Cruz, Santa Cruz, CA 95064, USA
[4] Istituto Nazionale di Fisica Nucleare, Sezione di Pisa, I-56127 Pisa, Italy
[5] Laboratoire AIM, CEA-IRFU/CNRS/Université Paris Diderot, Service d'Astrophysique, CEA Saclay, 91191 Gif sur Yvette, France
[6] Istituto Nazionale di Fisica Nucleare, Sezione di Trieste, I-34127 Trieste, Italy
[7] Dipartimento di Fisica, Università di Trieste, I-34127 Trieste, Italy
[8] Istituto Nazionale di Fisica Nucleare, Sezione di Padova, I-35131 Padova, Italy
[9] Dipartimento di Fisica "G. Galilei," Università di Padova, I-35131 Padova, Italy
[10] Department of Physics, Royal Institute of Technology (KTH), AlbaNova, SE-106 91 Stockholm, Sweden
[11] Department of Physics, Center for Cosmology and Astro-Particle Physics, The Ohio State University, Columbus, OH 43210, USA
[12] Laboratoire Leprince-Ringuet, École polytechnique, CNRS/IN2P3, Palaiseau, France
[13] Dipartimento di Fisica "M. Merlin" dell'Università e del Politecnico di Bari, I-70126 Bari, Italy
[14] Istituto Nazionale di Fisica Nucleare, Sezione di Bari, 70126 Bari, Italy
[15] Department of Physics, University of Washington, Seattle, WA 98195-1560; kerrm@u.washington.edu
[16] Columbia Astrophysics Laboratory, Columbia University, New York, NY 10027, USA
[17] INAF-Istituto di Astrofisica Spaziale e Fisica Cosmica, I-20133 Milano, Italy
[18] Istituto Nazionale di Fisica Nucleare, Sezione di Perugia, I-06123 Perugia, Italy
[19] Dipartimento di Fisica, Università degli Studi di Perugia, I-06123 Perugia, Italy
[20] George Mason University, Fairfax, VA 22030, USA
[21] NASA Goddard Space Flight Center, Greenbelt, MD 20771, USA
[22] Laboratoire de Physique et Chemie de l'Environnement, LPCE UMR 6115 CNRS, F-45071 Orléans Cedex 02, and Station de radioastronomie de Nançay, Observatoire de Paris, CNRS/INSU, F-18330 Nançay, France
[23] Laboratoire de Physique Théorique et Astroparticules, Université Montpellier 2, CNRS/IN2P3, Montpellier, France
[24] Department of Physics and Astronomy, Sonoma State University, Rohnert Park, CA 94928-3609, USA
[25] Department of Physics, Stockholm University, AlbaNova, SE-106 91 Stockholm, Sweden
[26] Agenzia Spaziale Italiana (ASI) Science Data Center, I-00044 Frascati (Roma), Italy
[27] National Radio Astronomy Observatory (NRAO), Charlottesville, VA 22903, USA
[28] Dipartimento di Fisica, Università di Udine and Istituto Nazionale di Fisica Nucleare, Sezione di Trieste, Gruppo Collegato di Udine, I-33100 Udine, Italy
[29] Istituto Universitario di Studi Superiori (IUSS), I-27100 Pavia, Italy
[30] CNRS/IN2P3, Centre d'Études Nucléaires Bordeaux Gradignan, UMR 5797, Gradignan, 33175, France; smith@cenbg.in2p3.fr, guillemo@cenbg.in2p3.fr
[31] Université de Bordeaux, Centre d'Études Nucléaires Bordeaux Gradignan, UMR 5797, Gradignan, 33175, France
[32] Jodrell Bank Centre for Astrophysics, School of Physics and Astronomy, University of Manchester, M13 9PL, UK
[33] Arecibo Observatory, Arecibo 00612, Puerto Rico
[34] Department of Physical Science and Hiroshima Astrophysical Science Center, Hiroshima University, Higashi-Hiroshima 739-8526, Japan

[35] University of Maryland, College Park, MD 20742, USA
[36] Australia Telescope National Facility, CSIRO, Epping, NSW 1710, Australia
[37] Department of Physics, Tokyo Institute of Technology, Meguro City, Tokyo 152-8551, Japan
[38] Cosmic Radiation Laboratory, Institute of Physical and Chemical Research (RIKEN), Wako, Saitama 351-0198, Japan
[39] UCO/Lick Observatories, Santa Cruz, CA 95064, USA
[40] Centre d'Étude Spatiale des Rayonnements, CNRS/UPS, BP 44346, F-30128 Toulouse Cedex 4, France
[41] Department of Physics, West Virginia University, Morgantown, WV 26506, USA
[42] Center for Research and Exploration in Space Science and Technology (CRESST), NASA Goddard Space Flight Center, Greenbelt, MD 20771, USA
[43] Istituto Nazionale di Fisica Nucleare, Sezione di Roma "Tor Vergata," I-00133 Roma, Italy
[44] Max-Planck Institut für extraterrestrische Physik, 85748 Garching, Germany
[45] Department of Physics and Astronomy, University of Denver, Denver, CO 80208, USA
[46] Institute of Space and Astronautical Science, JAXA, 3-1-1 Yoshinodai, Sagamihara, Kanagawa 229-8510, Japan
[47] Institut de Ciencies de l'Espai (IEEC-CSIC), Campus UAB, 08193 Barcelona, Spain
[48] NYCB Real-Time Computing Inc., Lattingtown, NY 11560-1025, USA
[49] Department of Chemistry and Physics, Purdue University Calumet, Hammond, IN 46323-2094, USA
[50] Institució Catalana de Recerca i Estudis Avançats (ICREA), Barcelona, Spain
[51] Consorzio Interuniversitario per la Fisica Spaziale (CIFS), I-10133 Torino, Italy
[52] Dipartimento di Fisica, Università di Roma "Tor Vergata," I-00133 Roma, Italy
[53] School of Pure and Applied Natural Sciences, University of Kalmar, SE-391 82 Kalmar, Sweden
Received 2009 January 16; accepted 2009 May 27; published 2009 July 8

ABSTRACT

We report the detection of pulsed gamma-rays from the young, spin-powered radio pulsar PSR J2021+3651 using data acquired with the Large Area Telescope (LAT) on the *Fermi Gamma-ray Space Telescope* (formerly *GLAST*). The light curve consists of two narrow peaks of similar amplitude separated by 0.468 ± 0.002 in phase. The first peak lags the maximum of the 2 GHz radio pulse by $0.162 \pm 0.004 \pm 0.01$ in phase. The integral gamma-ray photon flux above 100 MeV is $(56 \pm 3 \pm 11) \times 10^{-8}$ cm^{-2} s^{-1}. The photon spectrum is well described by an exponentially cut-off power law of the form $\frac{dF}{dE} = kE^{-\Gamma}e^{(-E/E_c)}$, where the energy E is expressed in GeV. The photon index is $\Gamma = 1.5 \pm 0.1 \pm 0.1$ and the exponential cut-off is $E_c = 2.4 \pm 0.3 \pm 0.5$ GeV. The first uncertainty is statistical and the second is systematic. The integral photon flux of the bridge is approximately 10% of the pulsed emission, and the upper limit on off-pulse gamma-ray emission from a putative pulsar wind nebula is $< 10\%$ of the pulsed emission at the 95% confidence level. Radio polarization measurements yield a rotation measure of RM $= 524 \pm 4$ rad m^{-2} but a poorly constrained magnetic geometry. Re-analysis of *Chandra X-ray Observatory* data enhanced the significance of the weak X-ray pulsations, and the first peak is roughly phase aligned with the first gamma-ray peak. We discuss the emission region and beaming geometry based on the shape and spectrum of the gamma-ray light curve combined with radio and X-ray measurements, and the implications for the pulsar distance. Gamma-ray emission from the polar cap region seems unlikely for this pulsar.

Key words: gamma rays: observations – pulsars: general – pulsars: individual (PSR J2021+3651)

Online-only material: color figures

1. INTRODUCTION

The Large Area Telescope (LAT) went into orbit on 2008 June 11 aboard the *Fermi Gamma-ray Space Telescope* (formerly *GLAST*; Atwood et al. 2009). Gamma-ray pulsations from the pulsar PSR J2021+3651 (Roberts et al. 2002) were detected during the first weeks of commissioning. The LAT was built to address, along with other pressing questions in high-energy astrophysics, the extent to which gamma-ray emission by pulsars is a rule, and thereby to better understand the mechanisms by which the kinetic energy of a rotating neutron star is transformed into intense beams of radiation. The discovery of a pulsed gamma-ray signal from PSR J2021+3651 was reported using *AGILE*, the "*Astro-rivelatore Gamma a Immagini LEggero*," by Halpern et al. (2008).

Following the detection of at least six high-energy gamma-ray pulsars by the Energetic Gamma Ray Experiment Telescope (EGRET) on the *Compton Gamma Ray Observatory* (see summary by Thompson 2004), observers sought positional coincidences of newly discovered pulsars (e.g., Kramer et al. 2003) with EGRET catalog sources (Hartman et al. 1999) or searched the EGRET error boxes for new radio pulsars (e.g., Crawford et al. 2006).

In one such search, Roberts et al. (2002) discovered PSR J2021+3651 with period 103.7 ms within the GeV error box associated with 3EG J2021+3716 (Lamb & Macomb 1997; Roberts et al. 2001). PSR J2021+3651 is young (characteristic timing age 17 kyr) and energetic ($\dot{E} = 3.38 \times 10^{36}$ erg s^{-1}). The NE2001 model (Cordes & Lazio 2002) for the Galactic distribution of free electrons for this line of sight ($l = 75\overset{\circ}{.}21$, $b = 0\overset{\circ}{.}13$) and the dispersion measure of DM ≈ 370 pc cm^{-3} suggests a distance of $D = 12$ kpc, with a fractional uncertainty that can exceed 50%. Subsequent investigations with the *Chandra X-ray Observatory* revealed a pulsar wind nebula (PWN) and possible pulsations in X-rays (Hessels et al. 2004). The torus of this "Dragonfly" PWN is clearly resolved, providing an estimate of the orientation of the pulsar's spin axis relative to the observer's line of sight of $85^\circ \pm 1^\circ$ (Van Etten et al. 2008). All authors point out that such a large distance implies high efficiency η for the conversion of spin-down power into gamma-rays, becoming unphysical ($\eta > 100\%$) for some beam scenarios, and explore different ways to constrain the distance. The X-ray spectra are consistent with a distance of 2–4 kpc. This paper adds new elements to the

[54] National Research Council Research Associate

discussion: a more detailed gamma-ray light curve with phase-resolved spectroscopy, a detailed comparison of the gamma-ray light curve with the predictions of various models, and radio polarization measurements.

PSR J2021+3651 illustrates the importance of sustained monitoring of pulsar timing. It is one of the more than 200 pulsars with $E > 10^{34}$ erg s^{-1} monitored by the program coordinated between the radio and X-ray timing community and the *Fermi* LAT team (Smith et al. 2008). PSR J2021+3651, like many young pulsars, exhibits timing noise. Not only does contemporaneous timing allow accurate comparisons between radio and gamma-ray light curves, but folding at a known period provides significantly greater sensitivity than searching for a periodicity. McLaughlin & Cordes (2004) detected significant periodicities for PSR J2021+3651 in two of eight EGRET viewing periods (VPs) containing the pulsar by extrapolating the timing solution and searching around a range of period and period derivative. The light curve was consistent between the two VPs and is similar to the LAT light curve. However, they were unable to detect significant pulsations in the other six VPs. PSR J2021+3651 was one of only two pulsars detected by them in this manner due to the large number of trials needed when extrapolating timing solutions back several years. The ongoing pulsar monitoring for *Fermi* greatly reduces such problems.

2. OBSERVATIONS

The LAT is a pair-production telescope. It consists of tungsten foil and silicon microstrip converter/trackers (pair conversion and track measurement); hodoscopic cesium iodide calorimeters (energy measurement); plastic scintillator anticoincidence detectors (charged-particle rejection); and a programmable trigger and data acquisition system. The LAT's excellent sensitivity stems from a large effective area (~ 8000 cm^2) and superior angular resolution. The broad field of view (2.4 sr) allows long exposures to the whole sky. The LAT is sensitive to gamma-rays with energy > 20 MeV. Verification of the on-orbit response is continuing but appears consistent with expectations.[55]

Gamma-ray events recorded with the LAT have timestamps that derive from a GPS clock on the *Fermi* satellite. Ground tests using cosmic ray muons demonstrated that the LAT measures event times with a precision significantly better than 1 μs. On orbit, satellite telemetry indicates comparable accuracy. Transformation to the solar system barycenter and phase calculations were done with the *Fermi* LAT "Science Tools," shown to be accurate to better than a few μs for isolated pulsars (Smith et al. 2008). Degradation of the barycentered time resolution from uncertainty in *Fermi*'s position is negligible. End-to-end performance of the timing systems was confirmed using the bright EGRET pulsars. The LAT gamma-ray phases of these pulsars relative to the radio phases agree with previous measurements (e.g., Fierro et al. 1998).

Data were acquired in two different *Fermi* observing modes. Between 2008 June 30 and August 3 the LAT was often pointed near the northern orbital pole ($\alpha = 18^{\rm h}40^{\rm m}$, $\delta = 60^\circ$, or $l = 90^\circ, b = 25^\circ$, in mid-July). Since then, *Fermi* has been scanning the entire sky every two orbits (approximately 3 hr). The data used here were acquired through 2008 November 15. The "diffuse" event selection was used ("Pass 6," ver. 1; see Atwood et al. 2009), leaving a background due to charged cosmic rays comparable to or less than the extragalactic diffuse gamma-ray emission. Gamma-rays with measured zenith angles greater than 105° were excluded, due to the intense gamma-ray emission from the Earth's limb caused by cosmic rays interacting in the atmosphere.

Table 1
Radio Ephemeris of PSR J2021+3651

Pulsar name	J2021+3651
Right ascension (J2000)[a]	20:21:05.46
Declination (J2000)[a]	36:51:04.8
Pulse frequency (s^{-1})	9.6393948581(3)
Frequency derivative (s^{-2})	$-8.89419(6)\times10^{-12}$
Frequency second derivative (s^{-3})	$1.09(5)\times10^{-21}$
Epoch of fit (MJD [TDB])	54710.0
Epoch of zero phase reference (MJD [TDB])[b]	54715.22791423678
Range of fit (MJD)	54634.18–54785.9
Dispersion measure (pc cm^{-3})[c]	367.5 ± 1

Notes. The digits in parentheses are the nominal 1σ TEMPO uncertainties.
[a] Celestial coordinates are from *Chandra* observations (Hessels et al. 2004).
[b] This is TEMPO's "TZRMJD" extrapolated to the solar system barycenter at infinite frequency.
[c] See Section 2 for details of this measurement.

PSR J2021+3651 is being observed by the timing consortium supporting *Fermi* observations with the NRAO Green Bank Telescope (GBT), the NAIC Arecibo telescope, and the Lovell telescope at Jodrell Bank. The combined usage of these observatories provides simultaneously good timing precision and good sampling. The most precise timing measurements are acquired at Arecibo and GBT, while the best sampling is obtained with GBT and Jodrell Bank; the observational setup at the latter is described in Hobbs et al. (2004). The WAPP spectrometer used at Arecibo is described in Dowd et al. (2000). Here we use a rotational ephemeris based on GBT data.

The phase-connected ephemeris for PSR J2021+3651 listed in Table 1, contemporaneous with the *Fermi* observations, was derived from 21 observations obtained between 2008 June 17 and November 15.[56] The DE405 solar system ephemeris was used (Standish 1998). The pulsar was observed at a center frequency of either 1950 MHz or 1550 MHz with the GBT Pulsar Spigot (Kaplan et al. 2005), yielding total power samples every 81.92 μs in each of 768 frequency channels over a bandwidth of 600 MHz. Each observation lasted for 5 minutes, from which we derived a time of arrival with typical uncertainty of 0.2 ms. PSR J2021+3651 exhibits rotational instability that is significant over the span of five months. We used the TEMPO timing software[57] and describe the pulsar rotation well by fitting for its frequency and first two derivatives. This timing solution had small unmodeled residual features ($\chi^2_\nu = 1.4$), with a post-fit rms of 0.2 ms. The DM is used to correct the time of arrival of the radio pulse to infinite frequency for absolute phase comparison with the gamma-ray profile. Because the radio profiles of PSR J2021+3651 are significantly scattered at the frequencies that we use for timing, an ordinary TEMPO fit biases the DM upward from its true value. In order to correct for this, we fit scattering models to the (assumed intrinsic) profile at 5 GHz until the resulting profiles matched the observed ones. The measured pulse broadening (scaled to 1 GHz) appears to be about a factor of 2 larger than previously estimated by Hessels et al. (2004). The corresponding DM $= 367.5 \pm 1$ pc cm^{-3} is 0.5% smaller than the value without this correction, where the estimated

[55] http://www-glast.slac.stanford.edu/software/IS/glast_lat_performance.htm

[56] This and other ephemerides used in *Fermi* results will be available from the Fermi Science Support Center (FSSC) data servers at http://fermi.gsfc.nasa.gov/ssc/data.

[57] http://www.atnf.csiro.au/research/pulsar/tempo/

uncertainty is dominated by systematic effects. The resulting phase uncertainty after extrapolation from 1.95 GHz to infinite frequency is ±0.01.

In addition to the Spigot observations, we observed the pulsar at 2000 MHz using the new Green Bank Ultimate Pulsar Processing Instrument (GUPPI)[58] at the GBT for 1.3 hr. GUPPI provides full-polarization spectra in 2048 channels over 800 MHz of bandwidth every 40.96 μs. The resulting data were polarization- and flux-calibrated based on observations of a local pulsed noise signal and the bright quasar J1445+0958. Analysis was performed using the PSRCHIVE software package (Hotan et al. 2004).

We re-analyzed the 20.8 ks *Chandra* ACIS-S continuous clocking data from MJD 52682 described in Hessels et al. (2004), using the current version of *Chandra* analysis software, and a timing solution built from near-contemporaneous radio observations acquired with the Lovell telescope at Jodrell Bank. The light curve is shown in Figure 1. The deviation from a flat light curve is slightly more significant (4.5σ) than that reported by Hessels et al. (3.7σ), has the same overall shape as their Figure 3, but is shifted in phase. The first peak seems to be within ≈ 0.1 in phase with the first gamma-ray peak albeit with weak statistics. Hessels et al. discussed the possibility of a nonthermal component from the X-ray point source, and Van Etten et al. measure this component's flux: the ratio of the X-ray nonthermal flux to the gamma-ray flux is 10^4, greater than that observed for Vela (10^3) or for Geminga (10^2; Bignami & Caraveo 1996). The X-ray light curve also resembles those of other established gamma-ray pulsars (Kaspi et al. 2006).

3. RESULTS

The LAT orientation with respect to the celestial sphere has been calibrated to a precision of 30″, using more than a dozen known bright point sources. The *Chandra*-derived position of PSR J2021+3651 is 0.′62 from the center of the gamma-ray 68% containment contour, which has a 0.′75 radius. Figure 2 shows the distribution of counts for the region surrounding the pulsar.

3.1. Light Curve

The top frame of Figure 1 shows the phase histogram for the gamma-ray events with energies >100 MeV, within an energy-dependent 68% angular containment radius of the radio pulsar position. There are two peaks: the first peak (P1) is the phase interval $0.13 < \phi < 0.20$, and P2 is $0.58 < \phi < 0.68$. Both peaks are well fit by a Lorentzian function, yielding full widths at half-maximum of 0.021 ± 0.002 and 0.053 ± 0.006 rotations, respectively, separated by $\Delta\phi_\gamma = 0.468 \pm 0.002$. P1 lags the maximum of the 2 GHz radio peak shown in the bottom frame by $\delta\phi_{\gamma\text{-radio}} = 0.162 \pm 0.004 \pm 0.01$ rotations of the neutron star. The first uncertainty is statistical; the second is due to the uncertainty in the DM. The intermediate frames show three energy bands: 100 MeV–1 GeV, 1–3 GeV, and >3 GeV. P1 fades with increasing energy, whereas P2 persists. The highest energy photon in this sample has 12 GeV, in P2. The peak positions are stable with energy to within 0.01 in phase.

3.2. Spectrum

The spectral shape, the cutoff energy, and the integral energy flux are observables that can be compared with pulsar emission models. PSR J2021+3651 is located in the Cygnus region

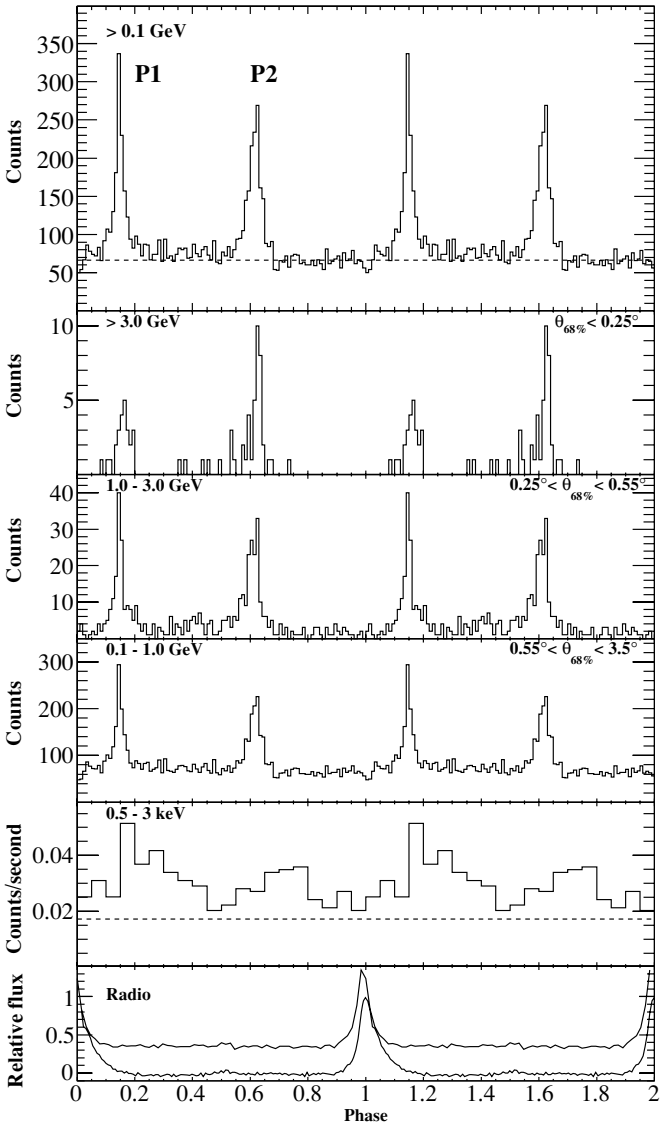

Figure 1. Top frame: light curve for PSR J2021+3651, for gamma-rays with energy >100 MeV within the energy-dependent 68% containment radius $\theta_{68\%}$ of the pulsar position. Each bin is 0.01 in phase, and two rotation cycles are shown. The horizontal dashed line shows the average number of counts in the off-pulse phase interval. Three following frames: light curves in the three indicated energy ranges. Second frame from bottom: phase-aligned *Chandra* ACIS-S CC X-ray light curve, with the background rate shown by the horizontal dashed line. Bottom frame: the upper curve is the 1950 MHz radio profile obtained using the Pulsar Spigot at the GBT. The lower curve is the total intensity profile obtained at Arecibo using the WAPP spectrometers with a 3.7 hr integration time and 300 MHz of bandwidth centered at 1500 MHz, vertically offset from the GBT curve for clarity. Both curves show evidence for an interpulse at phase 0.5 with amplitude ∼5% of the main pulse.

where diffuse emission is bright and there are poorly resolved neighboring sources (Figure 2). While most spectra in the third EGRET catalog were well modeled by a single power-law spectrum, 3EG J2021+3716 was a clear exception. A two power-law fit, with the break point fixed at 1 GeV, gave a reduced $\chi^2 = 0.55$, compared to reduced $\chi^2 = 2.8$ for the simple power law (Bertsch et al. 2000; Reimer & Bertsch 2001). The two spectral indices of 1.23 ± 0.15 and 3.39 ± 0.36 bracket the 3EG index of 1.86 ± 0.10. The integral photon flux of 35×10^{-8} cm^{-2} s^{-1} thus obtained is a bit more than half of the 3EG value, presumably because of how neighboring sources were handled. *AGILE* data confirm a spectral break near 2 GeV (Halpern et al. 2008).

[58] https://wikio.nrao.edu/bin/view/CICADA/GUPPiUsersGuide

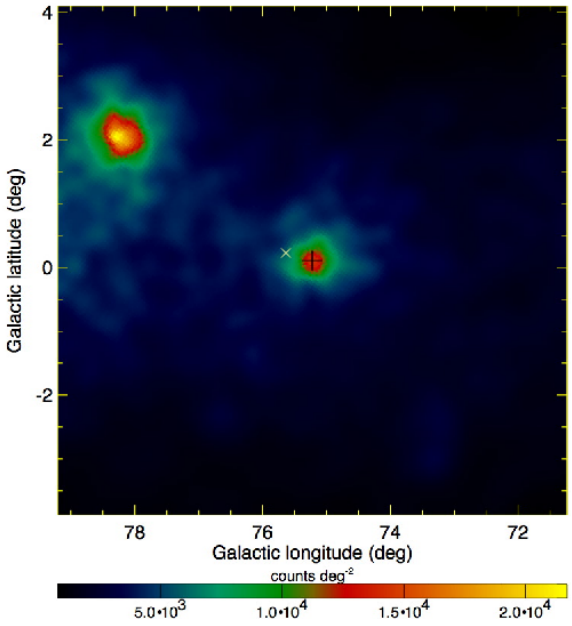

Figure 2. Gamma-ray counts per square degree, with $E > 100$ MeV, centered at the *Chandra*-derived position of PSR J2021+3651. Bin sizes vary such that statistical fluctuations are fixed to a signal-to-noise ratio of 10. The cross indicates the *Chandra*-derived position of PSR J2021+3651. The "X" indicates the position of the open cluster Berkeley 87. The bright object at upper-left is 3EG J2020+4017.

(A color version of this figure is available in the online journal.)

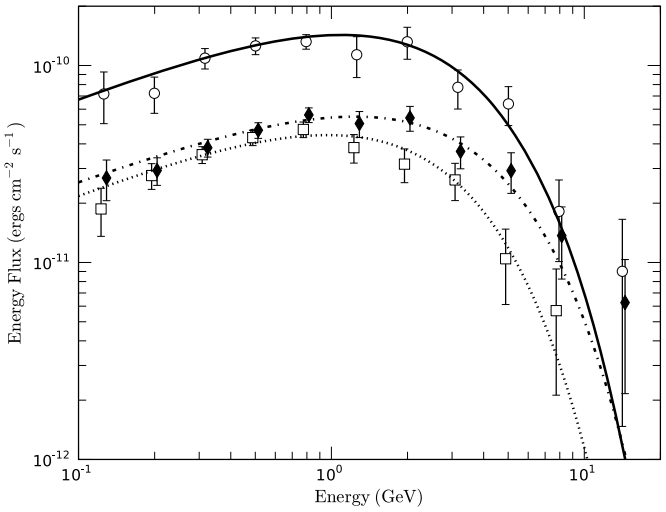

Figure 3. Spectral energy distribution E^2dF/dE for PSR J2021+3651 as fit by "gtlike" assuming a power-law spectrum with an exponential cut-off, for P1 (dotted), P2 (dot-dash), and total pulse (solid). The differential values as estimated by "on–off" are given for P1 (squares), P2 (diamonds), and total pulse (circles). The error bars are statistical only. For clarity, the points for P1 (P2) are plotted 2.5% lower (higher) in energy than for total pulse.

The different approaches used in analyses of LAT data to find the background contribution and to take into account the direction- and energy-dependent instrument response are outlined in our recent analysis of LAT data for Vela (Abdo et al. 2009). One method estimates the background and pulsar spectrum by maximizing the joint likelihood for the off-pulse data, phases $0.73 < \phi < 1.05$, and the pulsed data ("on–off"). Another models observed neighboring sources and the diffuse Galactic, extragalactic, and residual charged backgrounds, again in a likelihood approach ("gtlike," provided with the *Fermi* science tools). The "unfolding" method deconvolves the observed events from the instrument response. All three methods give consistent results.

Figure 3 shows the result of the likelihood fit to the data assuming a power-law spectrum with an exponential cutoff,

$$\frac{dF}{dE} = kE^{-\Gamma}e^{(-E/E_c)^b}$$

where the energy E is expressed in GeV and with $b = 1$, using only the on-pulse data ($0.05 < \phi < 0.73$). The curves are the "gtlike" results, whereas "on–off" gives a more faithful representation of the individual source data points, which are shown. To reduce confusion from the diffuse background and neighboring sources, we fit only photons above 200 MeV and extrapolate the result to 100 MeV. The spectral parameters are listed in Table 2, including the integral energy flux $h = (4.3 \pm 0.1) \times 10^{-10}$ erg cm^{-2} s^{-1} for $E > 100$ MeV. The Pearson χ^2 value for the fit is 1.1. Applying the likelihood ratio test against a spectral model with b left free, there is no evidence to reject the simple exponential model, a super-exponential cutoff ($b = 2$) is disfavored at the 3σ level, and a pure power-law ($b = 0$) is strongly excluded at 13σ.

We also measure the spectra of the two pulsar peaks individually. Applying the same background model and again imposing $b = 1$ yields the additional curves shown in Figure 3 and summarized in Table 2. P2 appears to persist to higher energies in Figure 1, and the fit results formally confirm this impression. However, in light of the systematic biases at play, the data are also consistent with no significant spectral difference between the two pulses. Bridge emission in the phase interval $0.26 < \phi < 0.54$ is apparent in Figure 1. It exceeds the backgrounds from the diffuse Galactic emission and from neighboring sources with 5σ significance, with a photon flux that contributes roughly 10% of the total on-pulse flux. Finally, the

Table 2
Spectral Results for PSR J2021+3651

Phase Interval	$\Delta\phi$	F^a (10^{-8} cm^{-2} s^{-1})	h^b (10^{-10} erg cm^{-2} s^{-1})	Γ	$E_c{}^c$ (GeV)
P1	0.13–0.20	18 ± 1	1.3 ± 0.1	1.5 ± 0.1	1.9 ± 0.3
P2	0.58–0.68	21 ± 1	1.7 ± 0.1	1.5 ± 0.1	2.8 ± 0.5
Bridge	0.26–0.54	≈10% of total pulse			
Total pulse	0.05–0.73	56 ± 3	4.3 ± 0.1	1.5 ± 0.1	2.4 ± 0.3
Off pulse	0.73–1.05	<10% of total pulse			

Notes.
[a] Integral photon flux (>100 MeV).
[b] Integral energy flux (>100 MeV). Flux systematic biases could lead to 20% increases, see the text.
[c] Energy of an exponential cut-off to a power-law spectrum with index Γ.

off-pulse data show no excess above the background, allowing us to place an upper limit on the flux of a putative gamma-ray PWN of <10% of the phase-averaged emission, at the 95% confidence level.

The uncertainties in Table 2 and above are statistical. Two effects dominate the systematic biases: modeling of the diffuse emission and neighboring sources over the several degree radius dictated by the point spread function at the lower energy bound; and uncertainties in the energy-dependent effective area. The latter is calculated using the test beam-verified Monte Carlo detector simulations (Baldini et al. 2007), and verified on-orbit using gamma-ray data from the Vela pulsar. For the LAT Vela spectral measurements (Abdo et al. 2009), the differences between observed and expected on-orbit gamma-ray efficiencies led to an uncertainty on the integral energy flux of $\pm\delta h/h = 20\%$. Since then, the differences have been found to arise from charge in the silicon tracker deposited by cosmic rays in a time window around the gamma-ray event. Gamma-ray event reconstruction and selection efficiencies below several hundred MeV are *smaller* than predicted, and the fluxes reported here will increase for future analyses taking the effect into account. The potential bias in the cutoff energy is of order ±0.5 GeV and that of the spectral index is $\delta\Gamma \approx 0.1$. The conclusion that the spectral shape for PSR J2021+3651 is most consistent with $b = 1$ is unaffected by these issues.

4. DISCUSSION

PSR J2021+3651 is among the first gamma-ray pulsars to be studied using *Fermi*. The gamma-ray observations, combined with X-ray images and spectra as well as with radio information such as polarization, allow stricter comparison with models than was previously possible. Improved knowledge of beam geometries will in turn aid interpretation of the number counts of radio-loud and radio-quiet gamma-ray pulsars that *Fermi* sees.

Emission models fall into two classes: polar cap (PC) scenarios (Daugherty & Harding 1996), which place the emission very close to the star surface and outer magnetosphere models. Of the latter, the outer gap (OG) picture (Romani & Yadigaroglu 1995; Cheng et al. 2000; Hirotani 2005) ascribes the double pulse to emission at the boundaries of a single magnetic pole, while the two pole caustic model (Dyks & Rudak 2003), a physical realization of which may be the modern version of the slot-gap (SG) picture (Muslimov & Harding 2004; Harding et al. 2008), assigns the two pulses to the trailing boundaries of separate magnetic poles.

Gamma-rays created at the polar caps interact with the intense magnetic fields near the neutron star surface, resulting in superexponential spectral cut-offs below a few gigaelectronvolts, while OG models predict simple exponential cut-offs. LAT confirms and refines the spectral break measured with EGRET and also seen with *AGILE* by Halpern et al. (2008). The observed emission beyond 10 GeV and absence of a sharp cut-off indicate outer magnetosphere processes.

From the phase separation of the peaks in the gamma-ray light curve $\Delta\phi_\gamma = 0.468$, lag from radio $\Delta\phi_{\gamma\text{-radio}} = 0.16$, and X-ray torus-derived viewing angle $\zeta = 85^\circ \pm 1^\circ$, we have bounds on the pulsar geometry that constrain the possible emission models. For the PC model $\Delta\phi_\gamma = 0.5$ is natural for large ζ and magnetic inclination α; one would expect to observe both radio pulses as well, since the observer must view the emission at a small angle $\beta = \zeta - \alpha$ to the magnetic pole to intersect the small PC beam. Indeed, Figure 1 shows a faint radio interpulse. On the other hand, both outer magnetosphere models can produce two narrow gamma-ray pulses at the observed separation for $\zeta = 85^\circ$. Narrow gamma-ray pulses arise naturally in outer magnetosphere models, where the peaks are formed by caustics. For OG and SG, a magnetic inclination of $\alpha \approx 70^\circ$ is inferred. For this α, the second radio pole may be faint ("grazing") or absent.

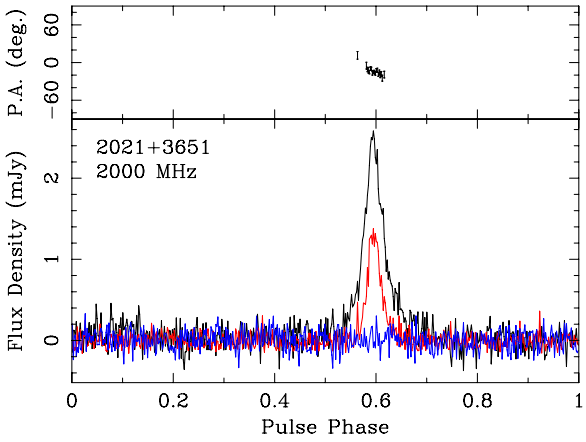

Figure 4. Bottom: polarization- and flux-calibrated profile for PSR J2021+3651 obtained with the GUPPI spectrometer at the GBT. The black trace corresponds to total intensity, the red to linear polarization, and the blue to circular polarization (greatest to least intensity at $\phi \approx 0.6$, respectively). The phase reference is different from Figure 1. The faint interpulse is visible near phase ≈ 0.1. Top: position angle of linear polarization, corrected to the pulsar frame, accounting for the Faraday rotation implied by the large rotation measure of RM = 524 ± 4 rad m^{-2}.

(A color version of this figure is available in the online journal.)

An additional radio observation supports the view that PSR J2021+3651 is a nearly orthogonal rotator, that is, has a large magnetic inclination. Figure 4 shows polarization data from which we determined the rotation measure (RM) of J2021+3651 to be 524 ± 4 rad m^{-2}, and measured the polarized pulse profile. The data are insufficient to constrain the parameters of the rotating vector model (RVM; Radhakrishnan & Cooke 1969): they are compatible with $\alpha \approx 70^\circ$ found above.

The large lag from the radio pulse is a challenge for simple versions of all models using a vacuum dipole magnetosphere. For the PC model we expect $\Delta\phi_{\gamma\text{-radio}} = 0$, in strong disagreement. Both the OG and SG models predict $\Delta\phi_{\gamma\text{-radio}} = 0.05$–0.1, for radio emission at the star surface. However, recent work (Johnston & Weisberg 2006; Karastergiou & Johnston 2007) suggests that radio emission from young, Vela-type pulsars occurs over a narrow range of altitudes below roughly 100 times the radius of the neutron star, whereas for their older brethren, it extends to lower altitudes. At high altitudes aberration shifts the radio pulse forward and widens the radio cone. If only the leading edge of the cone contributes to the narrow radio pulse, then the observed lag is easily achieved.

The emission scenarios predict different relations between the gamma-ray luminosity L_γ and the spin-down power $\dot{E}$, making the efficiency $\eta = L_\gamma/\dot{E}$ an additional discriminating observable, especially if applied to a large sample of gamma-ray pulsars. To obtain L_γ, the pulsar's distance D must be known, and the observed integral gamma-ray energy flux h must be extrapolated to the full sky, that is, some model of the beam shapes must be applied. In the past, the lack of geometric constraints for the small number of known gamma-ray pulsars led to the convention of simply assuming the gamma-ray beam

swept out a 1 sr solid angle, from which $L_\gamma = hD^2$; such a narrow beam is appropriate to near-surface polar cap emission. To better exploit the available data we define, following Watters et al. (2009), a correction factor f_Ω along the Earth line-of-sight ζ_E as

$$f_\Omega(\alpha, \zeta_E) = \frac{\int F_\gamma(\alpha; \zeta, \phi) \sin(\zeta) \mathrm{d}\zeta \, \mathrm{d}\phi}{2 \int F_\gamma(\alpha; \zeta_E, \phi) \mathrm{d}\phi} \quad (1)$$

such that

$$L_\gamma = 4\pi f_\Omega h D^2. \quad (2)$$

$F_\gamma(\alpha; \zeta, \phi)$ is the gamma-ray energy flux as a function of ζ and the pulsar rotation phase ϕ. In the ratio f_Ω, the numerator is the total emission over the full sky, and the denominator is the phase-averaged flux for the light curve seen from Earth. A 1 sr sky coverage corresponds to $f_\Omega = \frac{1}{4\pi} = 0.08$ and isotropic emission gives $f_\Omega = 1$. Note that $f_\Omega > 1$ is possible for beams that are narrow in ϕ, extended in ζ, and/or have average intensity exceeding the value sampled at ζ_E.

Polar cap models tend to have $f_\Omega \leqslant 0.1$, while for the fan beams of outer magnetosphere models f_Ω is much larger. For the OG model we estimate $f_\Omega \approx 1.05$ while the SG model has $f_\Omega \approx 1.1$ for the observed ζ (Watters et al. 2009).

The distance to PSR J2021+3651 is intriguing. The NE2001 electron density model assigns a distance of $12^{+\infty}_{-2.7}$ kpc to the large DM of the pulsar, but also greatly underestimates the measured scattering timescale, casting doubt on this inferred distance. Van Etten et al. (2008) placed the pulsar at $D = 2$ to 4 kpc, based on the PWN properties and the neutron star thermal emission. The large positive RM presented here is consistent with a distance at or beyond 4 kpc: of the nine pulsars within $\sim 10^\circ$ of this line of sight with measured RMs in the ATNF database[59] (Manchester et al. 2005), those with $D < 5$ kpc have negative RMs, while four others with $D \approx 6$–8 kpc have positive RM < 150 rad m^{-2} and DM from 130 to 240 pc cm^{-3}.

For a neutron star moment of inertia of 10^{45} g cm^2 we obtain

$$\eta = L_\gamma / \dot{E} = 0.25 f_\Omega (D/4 \text{ kpc})^2. \quad (3)$$

High-altitude models are preferred by the pulse and spectral shapes. A 25% efficiency is amongst the largest for all known gamma-ray pulsars, taking the f_Ω values as in Table 1 of Watters et al. (2009). The nominal DM distance imposes small f_Ω, i.e., polar cap emission, whereas the smaller distances imposed by the high-altitude models leave unexplained the large observed electron column density along the line of sight to the Dragonfly nebula.

The open cluster Berkeley 87 is 0.°5 from PSR J2021+3651. Prior to the pulsed gamma-ray detections, it was suspected to be a proton accelerator that could explain 3EG J2021+3716 and/or 3EG J2016+3657, and was searched for TeV emission (see e.g., Aharonian et al. 2006). The LAT localization clearly refutes Berkeley 87 as the dominant gamma-ray emitter in this direction, even if the off-pulse emission upper limit is near the intensity predicted by Bednarek (2007), leaving the door open for future explorations. The detailed maps in Schneider et al. (2007) include the position of PSR J2021+3651 and their re-examination may allow part of the large free electron column density to be accounted for.

[59] http://www.atnf.csiro.au/research/pulsar/psrcat/

5. CONCLUSIONS

PSR J2021+3651 was detected in gamma-rays in LAT data taken during *Fermi* instrument commissioning, with more data accumulated during the first few months of the all-sky survey. The extensive radio pulsar timing being performed for the *Fermi* mission facilitated the detection and enhanced the quality of the resulting light curves as well as their interpretation. Along with the discovery of a pulsed signal in the gamma-ray source CTA 1 identifying a previously mysterious source (Abdo et al. 2008), this is a good example of the remarkable capability of the LAT to identify Galactic sources. Of the 171 unidentified sources in the 3rd EGRET catalog, some 30 are Galactic ($|b| < 3^\circ$) and have steady fluxes as measured by EGRET. The identification of 3EG J2021+3716 suggests that many of these other sources could also be pulsars.

The high-resolution gamma-ray light curve, the faint radio interpulse, and the polarization data, together with earlier X-ray images of the torus and jet of the surrounding PWN, allow comparisons with different pulsar models. The rotation measure adds an argument in favor of an intermediate pulsar distance. Re-analysis of *Chandra* X-ray data yields an improved light curve. Phase-resolved spectral measurements show that both peaks cut off exponentially near 2 GeV. Gamma-ray emission from the polar cap is the least plausible explanation at present, even if the outer magnetosphere models imply large gamma-ray efficiencies if PSR J2021+3651 is indeed more distant than a few kiloparsec.

The *Fermi* LAT Collaboration acknowledges generous ongoing support from a number of agencies and institutes that have supported both the development and the operation of the LAT as well as scientific data analysis. These include the National Aeronautics and Space Administration and the Department of Energy in the United States, the Commissariat à l'Energie Atomique and the Centre National de la Recherche Scientifique/Institut National de Physique Nucléaire et de Physique des Particules in France, the Agenzia Spaziale Italiana and the Istituto Nazionale di Fisica Nucleare in Italy, the Ministry of Education, Culture, Sports, Science and Technology (MEXT), High Energy Accelerator Research Organization (KEK) and Japan Aerospace Exploration Agency (JAXA) in Japan, and the K. A. Wallenberg Foundation, the Swedish Research Council and the Swedish National Space Board in Sweden.

Additional support for science analysis during the operations phase from the following agencies is also gratefully acknowledged: the Istituto Nazionale di Astrofisica in Italy and the K. A. Wallenberg Foundation in Sweden for providing a grant in support of a Royal Swedish Academy of Sciences Research fellowship for JC.

The GBT is operated by the National Radio Astronomy Observatory, a facility of the National Science Foundation operated under cooperative agreement by Associated Universities, Inc. The Arecibo Observatory is part of the National Astronomy and Ionosphere Center (NAIC), a National Research Center operated by Cornell University under a cooperative agreement with the National Science Foundation.

REFERENCES

Abdo, A. A., et al. 2008, Science, 322, 1218
Abdo, A. A., et al. 2009, ApJ, 696, 1084
Aharonian, F. A., et al. 2006, A&A, 454, 775
Atwood, W. B., et al. 2009, ApJ, 697, 1071

Baldini, L., et al. 2007, in Proc. 1st GLAST Symp. 921, ed. S. Ritz, P. Michelson, & C. A. Meegan (Melville, NY: AIP), 190
Bednarek, W. 2007, MNRAS, 382, 367
Bertsch, D. L., et al. 2000, in Proc. 5th Compton Symp., ed. M. L. McConnell & J. M. Ryan (Melville, NY: AIP), 504
Bignami, G. F., & Caraveo, P. A. 1996, ARA&A, 34, 331
Cheng, K. S., Ruderman, M. A., & Zhang, L. 2000, ApJ, 537, 964
Cordes, J. M., & Lazio, T. J. W. 2002, arXiv:astro-ph/0207156
Crawford, F., Roberts, M. S. E., Hessels, J. W. T., Ransom, S. M., Livingstone, M., Tam, C. R., & Kaspi, V. M. 2006, ApJ, 652, 1499
Daugherty, J. K., & Harding, A. K. 1996, ApJ, 458, 278
Dowd, A., Sisk, W., & Hagen, J. 2000, in ASP Conf. Ser. 202, Proc. IAU Coll. 177, ed. M. Kramer, N. Wex, & N. Wielebinski (San Francisco, CA: ASP), 275
Dyks, J., & Rudak, B. 2003, ApJ, 598, 1201
Fierro, J. M., Michelson, P. F., Nolan, P. L., & Thompson, D. J. 1998, ApJ, 494, 734
Halpern, J. P., et al. 2008, ApJ, 688, 33
Harding, A. K., Stern, J. V., Dyks, J., & Frackowiak, M. 2008, ApJ, 680, 1378
Hartman, R. C., et al. 1999, ApJS, 123, 79
Hessels, J. W. T., Roberts, M. S. E., Ransom, S. M., Kaspi, V. M., Romani, R. W., Ng, C.-Y., Freire, P. C. C., & Gaensler, B. M. 2004, ApJ, 612, 389
Hirotani, K. 2005, Ap&SS, 297, 81
Hobbs, G., Lyne, A. G., Kramer, M., Martin, C. E., & Jordan, C. 2004, MNRAS, 353, 1311
Hotan, A. W., van Straten, W., & Manchester, R. N. 2004, PASA, 21, 302
Johnston, S., & Weisberg, J. M. 2006, MNRAS, 368, 1856
Kaplan, D. L., et al. 2005, PASP, 117, 643
Karastergiou, A., & Johnston, S. 2007, MNRAS, 380, 1678
Kaspi, V. M., Roberts, M. S. E., & Harding, A. K. 2006, in Compact Stellar X-ray Sources, ed. W. Lewin & M. van der Klis (Cambridge: Cambridge Univ. Press), 279
Kramer, M., et al. 2003, MNRAS, 342, 1299
Lamb, R. C., & Macomb, D. J. 1997, ApJ, 488, 872
Manchester, R. N., Hobbs, G. B., Teoh, A., & Hobbs, M. 2005, AJ, 129, 1993
McLaughlin, M. A., & Cordes, J. M. 2004, in X-ray and Gamma-Ray Astrophysics of Galactic Sources, ed. M. Tavani, A. Pellizzoni, & S. Vercellone (Rome: IASF), 67
Muslimov, A. G., & Harding, A. K. 2004, ApJ, 606, 1143
Radhakrishnan, V., & Cooke, D. J. 1969, Astrophys. Lett., 3, 225
Reimer, O., & Bertsch, D. L. 2001, Proc. of the 27th Int. Cosmic Ray Conf. 6, ed. M. Simon, E. Lorenz, & M. Pohl (Katlenburg-Lindau: Copernicus Gesellschaft), 2546
Roberts, M. S. E., Romani, R. W., & Kawai, N. 2001, ApJS, 133, 451
Roberts, M. S. E., Hessels, J. W. T., Ransom, S. M., Kaspi, V. M., Freire, P. C. C., Crawford, F., & Lorimer, D. R. 2002, ApJ, 577, L19
Romani, R. W., & Yadigaroglu, I.-A. 1995, ApJ, 438, 314
Schneider, N., et al. 2007, A&A, 474, 873
Smith, D. A., et al. 2008, A&A, 492, 923
Standish, E. M. 1988, JPL Planetary and Lunar Ephemerides, DE405/LE405, Memo IOM 312.F-98-048
Thompson, D. J. 2004, in Cosmic Gamma-Ray Sources, ed. K.S. Cheng & G. E. Romero (Dordrecht: Kluwer), 149
Van Etten, A., Romani, R. W., & Ng, C.-Y. 2008, ApJ, 680, 1417
Watters, K. P., et al. 2009, ApJ, 695, 1289